Miniaturized electromagnetic absorber for millimeter-wave RADAR systems

Geethanjali Govindarajan[1,2] · Gulam Nabi Alsath Mohammed[1] · Kirubaveni Savarimuthu[1] · Aruna Veeraselvam[3]

Abstract

This research investigates the design of a novel planar millimeter (mm)-wave absorber for RADAR application. The proposed mm-wave absorber is constructed using integrated and distributed elements to reduce the complexity of the design. The proposed absorber exhibits a dual resonance by exploiting the mutual coupling between two concentric square rings. The impedance matching is achieved by introducing corrugations between the square rings. The mm-wave absorber operates in the frequency range of 31.4–33 GHz (1.64 GHz) with a minimum absorptivity of 95–100%, respectively. The performance of the proposed absorber is demonstrated using equivalent circuit modelling. Owing to the symmetric nature of the unit cell, the proposed absorber offers stable performance for both TE and TM modes of operation. The prototype of the proposed absorber is fabricated on a single-layered FR-4 substrate with a thickness of $\frac{\lambda_0}{5.97}$ and periodicity of $\frac{\lambda_0}{1.91}$, where λ_0 is free space wavelength at the lowest resonant frequency. The observed result is validated using experimental measurements in free space and has good agreement with the simulated results. Hence, the proposed mm-wave absorber is a promising entity for stealth engineering in military and defense systems.

Keywords Absorber · Millimeter-wave · Metamaterial

1 Introduction

Radio detection and ranging (RADAR) is used for the detection and tracking of aircraft, spacecraft, ships, guided missiles, motor vehicles, and so on. RADAR transmits electromagnetic (EM) waves which are reflected by the metals in the aircraft. The aircraft metals are easily detected by the RADAR signals which require the need for EM absorbers on the aircraft. Anechoic chambers, electromagnetic compatibility control units, and concealment applications are some of the specified applications for EM absorbers.

✉ Gulam Nabi Alsath Mohammed
alsath@live.com

1   Department of Electronics and Communication Engineering, College of Engineering Guindy, Anna University, Chennai 600025, India

2   Department of Electronics and Communication Engineering, Sri Sivasubramaniya Nadar College of Engineering, Kalavakkam 603110, India

3   Department of Electronics and Communication Engineering, Panimalar Engineering College, Poonamallee, Chennai 600123, India

These absorbers are classified into three types such as wedge tapered absorbers, lossy absorbers, and metamaterial absorbers. The wedge-tapered absorbers, which are pyramidal-shaped, are arranged in an array to absorb the scattered electromagnetic waves in an anechoic chamber. Since these absorbers are bulky, they are undesired for portable applications. The lossy absorber is composed of material that uses either high permittivity or permeability with high absorptivity for wideband applications. Some of the absorbers achieve dual-band, multi-frequency bands, broadband. The metamaterial absorbers are artificially engineered electromagnetic structure that is composed of frequency-sensitive metal patterns developed on a dielectric substrate. Thus, researchers are interested in the development of absorbers for imaging, sensing, and stealth applications where the absorption of EM waves is of paramount importance. Amidst various purposes, this research work is focused on the design of a miniaturized metamaterial unit cell to focus on the needs of millimeter-wave stealth applications.

Stealth technology is termed as lower observable (LO) technology that provides a complete disappearance from the RADAR screen and is less likely to be targeted. In most stealth applications, the disappearance of the target

is implemented based on three different combinations such as applying paint to make it less visible and use Salisbury materials to nullify the effect by absorbing and exploiting the angles or curves to return the beam to the transmitter. This research is widely focused on the design of an EM wave absorber. The absorber for cloaking the EM waves must take a few considerations into account such as the change in the shape of the structure which affects the placement of the other devices, development cost, and change in the performance. These mm-wave absorbers are also used to reduce the RADAR signature and enhance the stealth aspects. The mm-wave absorbers are exploited to eliminate the undesired assailant radar signals. It can be designed to operate either in the narrowband or in the wideband which is based on the application requirement. However, the narrow bandwidth is limited due to its applications. Hence a wide bandwidth of absorption is achieved using multilayered structures [1], fractal structures, multi-resonance structures [2, 3], and using lumped elements [4, 5].

The study on the design and characteristics of absorbers in literature is discussed. In 2008, the metamaterial absorber was first introduced by Landy et al. [6]. Later, the researcher's interest is focused on the development of millimeter-wave absorbers for various applications. In Ref. [1], the researchers have proposed a microwave absorber that has 22 pairs of layers using two different dielectric materials and metals to achieve an ultra-wideband absorber. The size of the absorber in Ref. [1] is $2.31\lambda_{\text{eff}} \times 2.31\lambda_{\text{eff}}$ operating between 3.5 and 18.5 GHz with an absorptivity greater than 93%. The authors in Ref. [3] have reported a wideband flexible microwave absorber that is composed of resonant rings, chip resistors, and metal wires with a footprint of $0.77\lambda_{\text{eff}} \times 0.77_{\text{eff}}$. The reported absorber operates between 2.55 and $10.0\lambda7$ GHz with an absorptivity of greater than 90% using an air gap of 9.9 mm thick between the dielectric and the bottom metal plate. In Ref. [7], the researchers have proposed an E-shaped fractal-based metallic splitting-ring resonator with a footprint of $3.66\lambda_{\text{eff}} \times 3.66\lambda_{\text{eff}}$ which achieves absorptivity of 80% between 20 and 30 GHz. An absorber with a metallic resonance structure that consists of two overlapping squares is designed in Ref. [8], with a footprint of $3.89\lambda_{\text{eff}} \times 3.89\lambda_{\text{eff}}$. The reported absorber obtains a minimum absorptivity of 80% from 20.59 to 43.73 GHz. The polarization sensitivity for pairs of angles such as 0° and 90°, 15° and 75°, and so on are discussed. A novel ultra-thin polarization-independent metamaterial absorber that operates for a triple-band is presented in Ref. [9]. The absorber is characterized by using narrow bandwidth, with a minimum absorption of 90% at 24 GHz. The researchers in Ref. [10] proposed millimeter-wave absorbers using various metals and dielectric constants. Since the research works on absorbers at the desired frequency range (31.4–33.04 GHz)

for RADAR application are limited, the literature on different frequency ranges is considered.

In alignment with the aforementioned research various structures utilizing dual substrates [1], lumped elements, PIN diodes [3], high profile [11], and narrow bands [9], metasurfaces [12] have been presented. However, achieving a single band with higher absorption is a challenging task. To the best of the author's knowledge, most of the absorbers presented in the works of literature have used higher profile [1–3, 11] to improve the bandwidth enhancement. A linearly polarized mm-wave absorber regime is proposed. The absorber's bandwidth is enhanced by only using distributed elements such as slots and stubs. The mm-wave absorber offers a high absorptivity of 95–100% by integrating square ring resonators in a single PCB layer. The proposed absorber exhibits a stable performance in TE and TM mode, which portrays polarization-insensitive behavior. A prototype of 40×40 cells is fabricated and tested using a lab-made experimental setup exploiting high-frequency pyramidal absorbers. Good agreement between the experiment and simulated result is observed. Thus, the proposed mm-wave absorber lowers the RCS and eliminates the undesired RADAR signals. Hence, the proposed mm-wave absorber is a promising entity for RADAR and military applications. The manuscript is prearranged as follows. The design, characterization, and performance of the proposed absorber are presented in Sect. 2, while the polarization stability is examined in Sect. 3. The fabrication, measurement, and angular stability of the proposed absorber are discussed in detail in Sect. 4. The simulated and measured results are discussed and analyzed in Sect. 5.

2 Absorber principle

The proposed mm-wave absorber is suitable for the RADAR application since it works in the RADAR frequency range (31.4–33 GHz) as recommended by Federal Communication Commission (FCC). The proposed absorber significantly reduces the RADAR cross-section and shields the electronic components and structures from electromagnetic waves []. The unit cell is designed by exploiting the distributed elements and achieves a minimum absorptivity of 95% throughout the operating bandwidth. In this work, an mm-wave absorber is presented using a dual resonance structure that consists of concentric square rings with corrugations in between the square rings. The design of a novel single-layer mm-wave absorber is discussed in this segment.

2.1 Construction

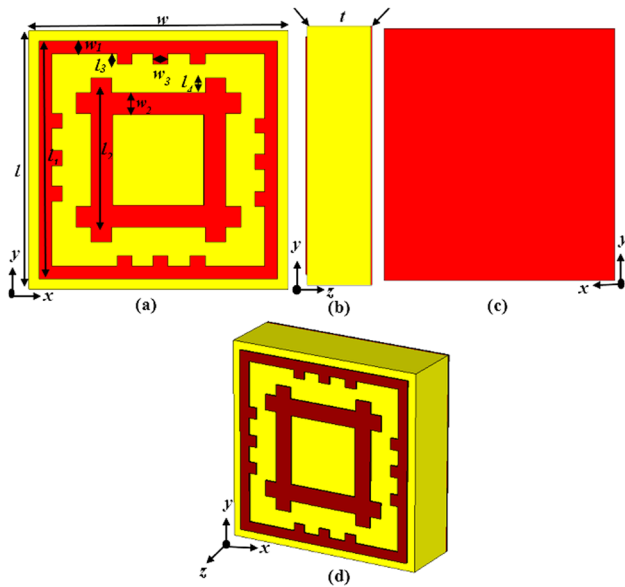The geometry of the proposed mm-wave absorber is shown in Fig. 1. The footprint of the proposed absorber is

Fig. 1 Geometry of the proposed mm-wave absorber from **a** front view, **b** side view, **c** back view, **d** perspective view

Fig. 2 ECM of the proposed absorber. The approximate circuit parameters are Cgs (dielectric) = 0.1 pF, L_1 = 2.594 nH, C_1 = 1.4 pF, L_2 = 2.401 nH, C_2 = 10.40 pF

5 mm × 5 mm (0.090 λ_0). The top conducting layer of the mm-wave absorber has a single resonance structure using two concentric square rings. The corrugations are created between the square rings which are facing each other as shown in Fig. 1a. Figure 1b, c illustrate the side and back views of the proposed absorber, respectively. Figure 1d represents the perspective view of the proposed absorber. The lossy 1.6 mm thick FR-4 substrate with a dielectric constant of 4.3 and loss tangent of 0.025 is used for the further development of the absorber. The top metallic layers are created using copper annealed with a thickness of 0.035 which has a frequency-dependent conductivity of 5.8×10^7 S/m. Table 1 shows the optimized dimensions for the proposed mm-wave absorber. The full-wave 3D electromagnetic solver, CST Microwave Studio Suite 2018, is used to simulate, characterize and optimize the proposed absorber.

Figure 2 constitutes the equivalent circuit model (ECM) for the proposed absorber. The values of the inductance and capacitance are calculated by using the theoretical LC component network analysis explained in Ref. [13]. The comparison between the equivalent circuit model and the simulated
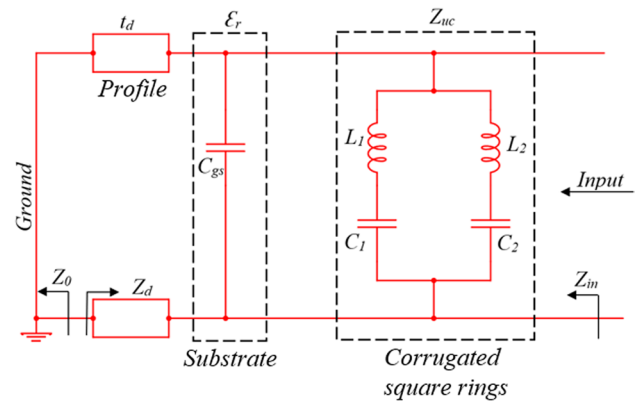
result is shown in Fig. 3. It is developed and the values are verified by using ADS software.

The proposed mm-wave absorber is analyzed based on the reflection (R), absorption (A), and transmission (T) characteristics. The finite integration technique in CST, which adapts the Floquet mode theory is used to investigate the characteristics of the absorber. The uniform plane wave excitation is used to study the reflection and transmission properties of the proposed absorber. The electromagnetic wave is defined along the z-direction, while the periodic boundary conditions are defined along the 'x' and 'y' directions. The x and y direction represents the unit cell where Z_{min} and Z_{max} are set to $E_t = 0$ and open to free space, respectively.

According to Munk's theory [14], the equivalent circuit of the double square ring (DSR) is identical to the LC series resonance. This circuit exhibits a band stop characteristic and 0% transmission [3]. In the modified ECM, Z_d represents the impedance provided by the dielectric substrate and t_d is the thickness of the substrate. Furthermore, modelling the substrate results in a transmission line with an appropriate characteristic impedance. The Floquet mode theory in the analysis of subwavelength elements [15, 16], which are used in the periodic arrays to design the unit cell. Electromagnetic wave absorption is widely explained with the help of impedance matching in the design of the absorber. The dielectric impedance (Z_d) and the unit cell impedance (Z_{uc}) are used to compute

Table 1 Dimension details of the proposed mm-wave absorber

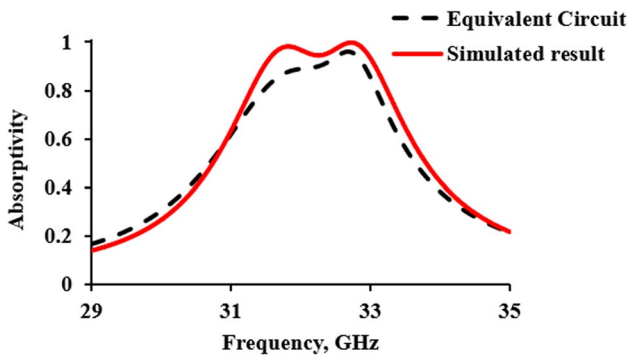| Parameters	l	w	l_1	w_1	l_2	w_2	t
Value (mm)	5	5	4.6	0.25	3.18	0.4	1.6
Parameters	l_3		w_3		l_4		w_4
Value (mm)	0.29		0.2		0.29		0.4

Fig. 3 Comparison of equivalent circuit performance and simulated result

the absorber's effective input impedance. The dielectric impedance is calculated using Eq. (1) [17].

$$Z_d = \frac{Z_0}{\sqrt{\varepsilon_r}} \tan(\beta t_d),$$ (1)

where Z_0 denotes the characteristic impedance, β represents the propagation constant, and t_d denotes the thickness of the substrate. The unit cell impedance is evaluated from the effective inductance and effective capacitance by using Eq. (2).

$$Z_{in} = Z_{uc}||Z_d$$ (2)

Therefore, it is required to match the absorber impedance Z_{in} with the free space impedance Z_0 using Eq. (3), where Γ is the reflectance [3].

$$\Gamma = \frac{(Z_{in} - Z_0)}{(Z_{in} + Z_0)}$$ (3)

The real part of the impedance of the absorber needs to be close to Z_0 i.e., 377 Ω and its imaginary part should be zero for minimum reflection and maximum absorption. It is known as the free space impedance $Z_0 = \sqrt{\mu_0/\varepsilon_0}$. Therefore, the absorption of the incident electromagnetic wave is maximized by controlling the resonance of μ and ε. In the proposed mm-wave absorber, the metallic structure and metal surface decide the equivalent capacitance and inductance which determines the resonant frequency (ω_0) using Eq. (4).

$$\omega_0 = \frac{1}{\sqrt{LC}}$$ (4)

The scattering parameters are used to calculate the overall absorption. Thus, the power absorbed is calculated using the following expressions [2].
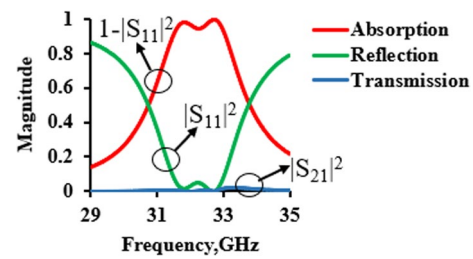
$$A(\omega) = 1 - T(\omega) - R(\omega)$$ (5)

Fig. 4 Absorption, reflection, and transmission characteristics of the proposed absorber

$$A(\omega) = 1 - |S_{21}(\omega)|^2 - |S_{11}(\omega)|^2$$ (6)

where

$$|S_{11}(\omega)|^2 = |S_{11_{xx}}(\omega)^2| + |S_{11_{yx}}(\omega)|^2$$ (7)

where the subscript '*xx*' represents co-components and '*yx*' represents cross-components. The cross-component vanishes in this proposed absorber and thus Eq. (7) is changed to Eq. (8).

$$A(\omega) = 1 - |S_{11_{xx}}(\omega)|^2$$ (8)

The absorption, reflection, and transmission characteristics are plotted in Fig. 4. Due to the presence of ground beneath the FR-4 substrate where $S_{21}(\omega) = 0$ and thus $T(\omega) = 0$. This prevents the incident EM wave to propagate on the rear side of the proposed mm-wave absorber. From the figure, it is inferred that the proposed absorber shows zero transmission characteristics, a minimum reflection of about 10%, and high absorption in the frequency range of 31.4–33 GHz. When the absorber is paired with the free space, most of the energy of the EM waves is coupled to the absorber and then the energy is consumed through dielectric loss and square rings.

2.2 Evolution

The stages of development of the proposed mm-wave absorber are shown in Fig. 5. The absorption characteristics of the concentric square rings show an absorption spectrum from 31.4 to 34 GHz as shown in Fig. 5a. The wide bandwidth of 2.6 GHz is obtained with minimum absorption is 60%. Further, to improve the absorption level, the inductance effect is increased where the inductance value is determined by the LC resonance circuit using the following Eq. (9).

$$f_r = \frac{1}{2\pi\sqrt{LC}}$$ (9)

The metallic patterns contribute to the circuit inductance and the gap between the concentric rings and offer the
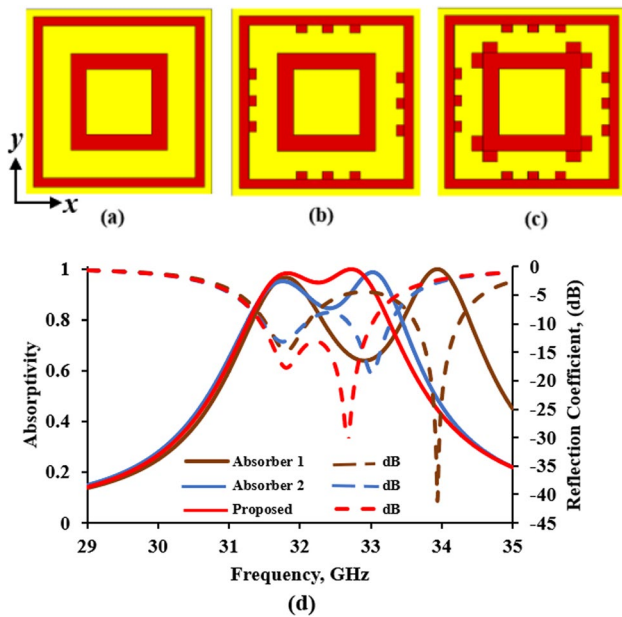
Fig. 5 Various stages of development of the designed absorber **a** absorber 1, **b** absorber 2, **c** proposed absorber, and **d** evolution of the proposed absorber in absorptivity and reflection coefficient

capacitance effect. The inductance is improved by incorporating the stubs of width 0.2 mm, to the outer square ring in the appropriate location for impedance matching as shown in Fig. 5b. Thus, the minimum absorptivity is improved to 78% by compromising the bandwidth. Figure 6a shows the bandwidth attained from 31.4 to 33.1 GHz. It is inferred from Fig. 5c, the absorptivity of absorber 2 is increased by lowering the capacitance between the two concentric square rings and incorporating stubs. The primary reason for the decreased resonance frequency is the presence of parasitic inductance in the capacitance. Thus, the desired absorption characteristics for the bandwidth of 1.64 GHz (31.4–33.04 GHz) as specifically mentioned by the FCC for airborne RADAR applications are achieved to minimize the
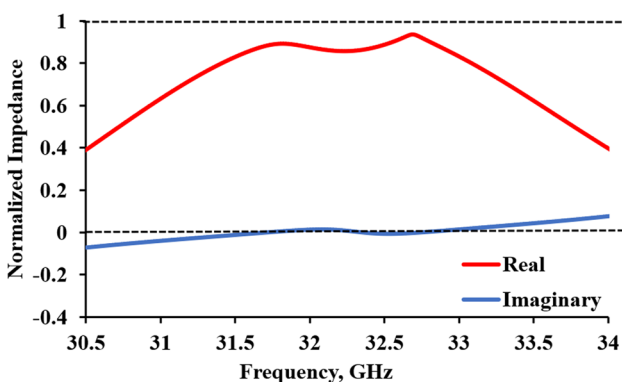
interferences between the stations in the radio navigation service. The evolution of proposed absorber for absorption and reflection characteristics are shown in Fig. 5d. It is inferred that, the absorptivity of the single-layered mm-wave absorber is achieved by the optimized inductive element in the appropriate position. Hence the impedance is matched to obtain a − 10 dB reflection coefficient.

This reduction in reflection increases the level of the absorption throughout the entire desired frequency range. The absorption mechanism of the proposed absorber can be realized with the help of the normalized impedance as shown in Fig. 6. It is inferred that the absorption peak of the real value of the normalized input impedance is close to unity while the imaginary part is zero, implying perfect impedance matching under free space conditions $(377 + j0)$. Thus, the realized reflection is minimum while the absorption is close to unity. The relative impedance (z_r) can be calculated using [18].

$$z_r = \pm \sqrt{\frac{\left(1 + s_{11}\right)^2 - s_{12}^2}{\left(1 - s_{11}\right)^2 - s_{12}^2}} \qquad (10)$$

The transmission coefficient $(|S_{12}|)$ for the proposed absorber is zero due to the presence of the full ground plane. Thus the impedance equation is given as,

$$z_r = \pm \sqrt{\frac{\left(1 + s_{11}\right)^2}{\left(1 - s_{11}\right)^2}} \qquad (11)$$

2.3 Loss performance of the substrate

The absorption characteristics of the proposed mm-wave absorber are analyzed for both lossy and lossless characteristics of the substrate and the results are presented in Fig. 7. It is inferred from the figure that the lossless FR-4 substrate has a very low absorptivity of 20% at 32.7 GHz with narrow bandwidth compared to the lossy FR-4 substrate. Also, the loss tangent is very small for a good dielectric material with
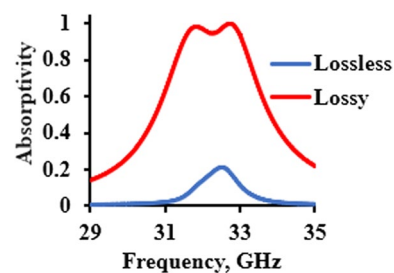

Fig. 6 Normalized impedance of the proposed absorber

Fig. 7 Loss performance of the proposed absorber

very small conductivity at high frequency which is evident from Eq. (10). These characteristics improve the level of absorption for the proposed absorber. Thus, considering the dissipation factor and material loss of the FR-4 material, the proposed absorber is designed for high frequency with maximum absorptivity for airborne application.

$$\tan \delta = \frac{\sigma}{\omega \varepsilon} \tag{12}$$

2.4 Parametric analysis

The proposed mm-wave absorber is further examined for different design parameters such as the height of the substrate (t) and length of the stub (L_4). The absorption characteristics for the above-mentioned parameters are analyzed and reported as shown in Fig. 8a, b. The height of the substrate (t) is an important parameter to obtain a maximum absorptivity of 100% at the desired bandwidth. The height of the substrate is optimized to $t = 1.6$ mm, whereas lesser absorptivity is obtained for $t = 1.2$ mm and a redshift in frequency occurs for $t = 1.8$ mm with reduced bandwidth as depicted in Fig. 8a. The performance of the absorber is analyzed for various lengths of the stub (L_4) at the inner square ring as discussed in Sect. 2.1. The length of the stub is optimized to 0.29 mm for best absorptivity with wide bandwidth. The reduced length of the stub (0.19 mm) results in a minimum absorptivity of 85% and even the bandwidth is improved to 1.7 GHz. In case, the stub length is further extended to 0.39 mm, the least absorption is improved with reduced bandwidth of 1.56 GHz as shown in Fig. 8b.

3 Stability analysis

This section evaluates and describes the proposed absorber's polarization stability. The steadiness of polarization at the normal incidence i.e., $\theta = 0°$, is analyzed for transverse electric (TE) mode with $\phi = 0°$ and transverse magnetic (TM) mode with $\phi = 90°$. As shown in Fig. 9, the rotational geometry of the proposed mm-wave absorber provides identical

Fig. 9 Characteristics of polarization for the designed mm-wave absorber

absorption characteristics in both TE and TM modes of operation. To further, analyze the stability of polarization, the surface plasmon density for the resonant frequency of 32.5 GHz is illustrated in Fig. 10. For the TE mode, the outer corrugated square ring is the primary reason for the absorption peak in the first resonance frequency. Thus, the current distributes in the horizontal arms which are depicted in Fig. 10a. Similarly, for the TM mode of propagation, a high plasmon density is observed along the vertical arm of the outer square loop, as shown in Fig. 10b. This signifies the polarization-insensitive behavior of the designed mm-wave absorber for incoming electromagnetic waves.

To further describe the resonant characteristics, the surface current density of the proposed mm-wave absorber is analyzed for resonant frequencies such as 31.4 GHz, 32.5 GHz, and 33 GHz. The surface plasmon density is investigated for TE mode under normal incidence. Figure 11a depicts the current flow at the outer metallic loop. The corrugations are introduced to the outer square loop to increase the impedance performance. Thus, the current distribution is strong in the outer corrugated ring which obtains the higher absorptivity at 31.4 GHz. The coupling between the outer ring and inner corrugated ring gives the minimum absorptivity of 95% in the resonant frequency of 32.5 GHz which is illustrated in Fig. 11b. The main cause for the peak resonance at 33 GHz is the combination of the outer and
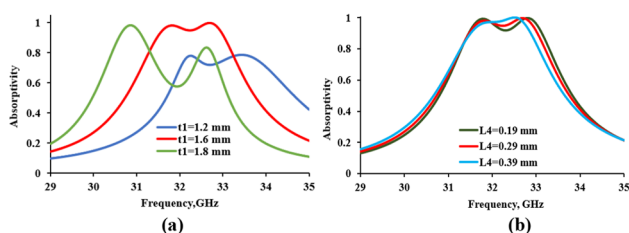
Fig. 8 **a** Performance of the proposed absorber for different substrate thicknesses, **b** characteristics of absorption for various lengths of the stub at the inner square ring (L_4)
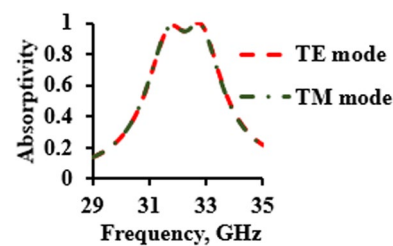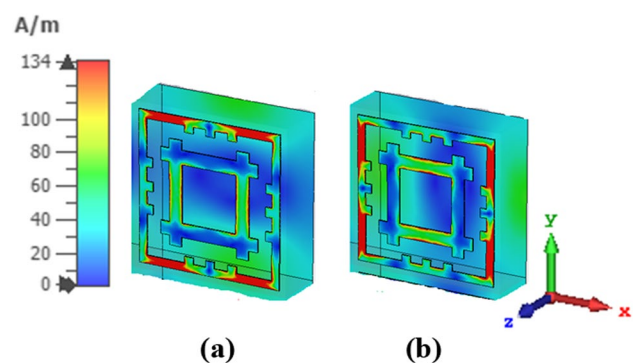
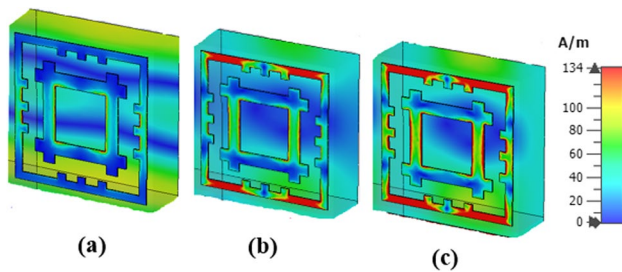**Fig. 10** Surface plasmon density of **a** TE mode and **b** TM mode

Fig. 11 Surface current density at **a** 31.4 GHz, **b** 32.5 GHz, **c** 33.04 GHz

inner corrugated square rings. It is inferred from Fig. 11c, the current distribution is strong in the edges of the square rings which gives the maximum absorptivity in the higher resonant frequency.

4 Fabrication and measurement

4.1 Fabrication

The proposed mm-wave absorber is fabricated and tested in the free space. Figure 13 displays an array of 40×40 cells fabricated on the FR-4 substrate with a thickness of 1.6 mm, size of 200 mm × 200 mm, and permittivity of 4.3. The fabricated prototype is a periodic arrangement of the proposed unit cells as illustrated in Fig. 12.
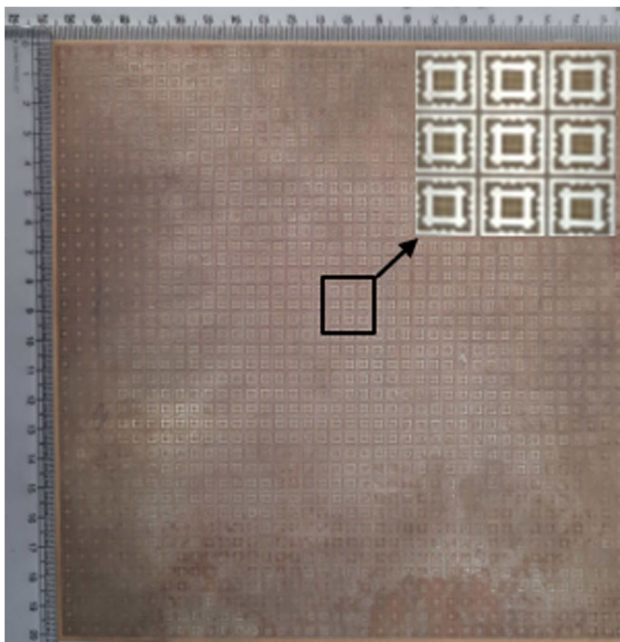

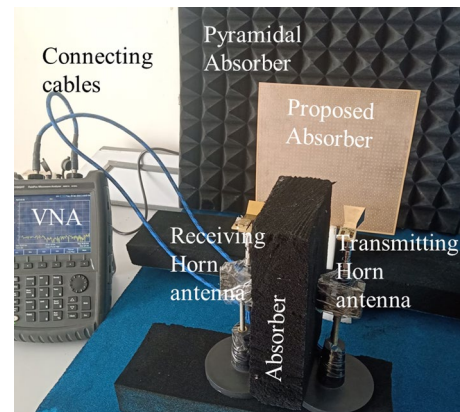**Fig. 12** Fabricated proposed mm-wave absorber with a magnified view

Fig. 13 Measurement set-up for the proposed absorber

4.2 Measurement

The performance of the proposed absorber is measured using a pair of high-frequency transmit and receive (T/R) horn antennas connected to the Vector Network Analyzer (VNA) (Keysight N9951A). The VNA (300 kHz–44 GHz) is calibrated initially fixing the operating frequency range and power level. The T/R horn antennas are separated using polyurethane foam to minimize the electromagnetic coupling at the intended frequency. The measurement setup is shown in Fig. 13. During the measurement, the fabricated prototype is placed in the far-field region of the antenna. The background noise is measured using the VNA without placing the sample in the measurement setup. The reflectivity of a full copper metal plate of the same dimension is measured. The copper plate is then replaced with the fabricated absorber, and the reflection coefficient is determined. The difference in reflection coefficients of the metal plate and the absorber prototype is used to calculate the actual reflection coefficient of the fabricated absorber. The measured and the simulated absorption characteristics show a good agreement from 31.4 to 33.6 GHz and a bandwidth of 2.2 GHz as shown in Fig. 14. The ripples are caused by impedance mismatch and it is partially due to the measurement error inventive of random noises in the environment. The performance of the reflection coefficient changes in the higher frequency band due to high-frequency EM wave diffraction at the prototype's edges. Nevertheless, the absorber performance in simulation and measured results are preferably consistent.

Thus, the proposed electromagnetic absorber is a suitable candidate for mm-wave RADAR applications. Table 2 shows the performance comparison with the other relevant absorbers. From the comparison, it is observed that the proposed absorber is designed exclusively for stealth applications at the frequency range of 31.4–33.04 GHz, with the highest minimum absorption of 95% throughout the bandwidth of 1.64 GHz. The size of the proposed absorber
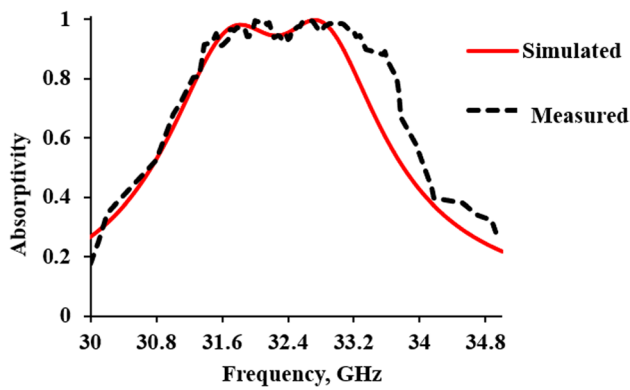
Fig. 14 Simulated and measured absorptivity of the proposed mm-wave absorber

is smaller by 53.68%, 70.76%, 71.08%, and 53.28%, and of [1, 3, 19, 20], respectively. The research on the development of the single band with dual resonant mm-wave absorbers at the intended RADAR frequency (30–33 GHz) is limited. The following important inferences are obtained based on this comparison table:

1. In comparison with the unit cell size of the reported absorbers in Refs. [1, 8, 19–23], the proposed absorber achieves miniaturization of 81%, 90%, 92.6%, 80%, 57%, 55%, and 65%, respectively.
2. The reported works [8, 24] have obtained a narrow bandwidth of < 0.2 GHz and < 0.15 GHz which is low compared to the proposed bandwidth (1.64 GHz).
3. The reported bandwidths (< 1.55 GHz) of [23, 24] are obtained by utilizing the maximum no. of lumped resistors. However, without the incorporation of lumped ele-

ments, the proposed absorber achieves a bandwidth of 1.64 GHz in the frequency range of 31.4–33 GHz.

4. By implementing the lumped elements in Refs. [23, 25] the reported absorptivity (< 93.1%) is low as the proposed absorber (95%). The usage of lumped elements leads to more complexity in the realization of precise impedance matching value and soldering of the lumped resistors.
5. The dual substrate, chess configuration, and multiple layers are utilized in Refs. [1, 19, 20, 22] to obtain a wider bandwidth and higher absorptivity which portrays the periodicity of the reported absorbers as large and bulky.
6. The novel unit cell used in the proposed absorber design offers a higher absorption of 95–100% over a wide frequency range of 31.4–33 GHz which is more than the absorptivity obtained in Refs. [1–3, 7, 19–21].

Figures 15 and 16 show the absorption characteristics for various oblique incidences under TE and TM modes. Thus, it is inferred from the figure that the increase in oblique incidence decreases the absorption performance owing to the shorter wavelength. Due to the high operating frequency, the performance of the absorber changes at higher angles of the incidence [26]. The variation is also attributed to the reduced tolerance of the slots and stubs in the absorber layout. The deterioration of the magnetic flux between the top and bottom metallic layers as the angle of incidence (θ) increases provides a predominant electric resonance and turns into a mismatching impedance [27]. Besides, the proposed absorber still maintains a good performance in both TE and TM modes with a minimum absorption of 92%, when θ is less than 30º.

Table 2 Performance comparison with other relevant absorbers

| References	Size ($\lambda_{eff} \times \lambda_{eff}$)	Operating frequency (GHz)	Bandwidth (GHz)	Thickness of substrate (mm)	Methods used to obtain the bandwidth	Minimum Absorption (%)	Percentage size reduction (%)
[1]	2.31 $\lambda_{eff} \times$ 2.31 λ_{eff}	3.5–18.5	15	18.7	Dual substrate	93	81
[8]	3.89 $\lambda_{eff} \times$ 3.89 λ_{eff}	2.5, 6, 11.2	–	1.5	Via holes	90	90
[19]	3.70 $\lambda_{eff} \times$ 3.70 λ_{eff}	14.5–21.8	7.3	1.27	Chessboard	80	92.6
[20]	2.29 $\lambda_{eff} \times$ 2.29 λ_{eff}	15–16	1	1.27	Chessboard	90	80
[28]	0.75 $\lambda_{eff} \times$ 0.75 λ_{eff}	3.5–5.5	3	8	Lumped elements	85	–
[25]	0.45 $\lambda_{eff} \times$ 0.45 λ_{eff}	8–9.5	1.5	3.2	Lumped resistors	90	–
[24]	1.03 $\lambda_{eff} \times$ 1.03 λ_{eff}	6, 9	–	1.5	Lumped resistors	95	57
[21]	1.5 $\lambda_{eff} \times$ 1.5 λ_{eff}	3–5	2	3	Lumped resistors	89	55
[22]	1.0 $\lambda_{eff} \times$ 1.0 λ_{eff}	6–8.5	2	2	Multiple layers	90	–
[23]	1.7 $\lambda_{eff} \times$ 1.7 λ_{eff}	6.1–7.4	1.3	6	Lumped elements	93	65
This work	1.07 $\lambda_{eff} \times$ 1.07 λ_{eff}	31.4–33.04	1.64	1.6	Distributed elements in a single PCB layer	95	–
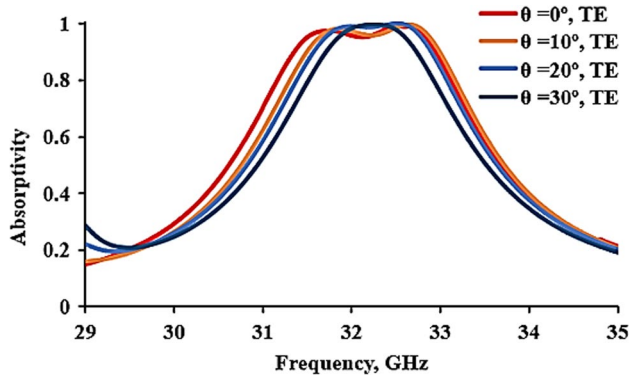
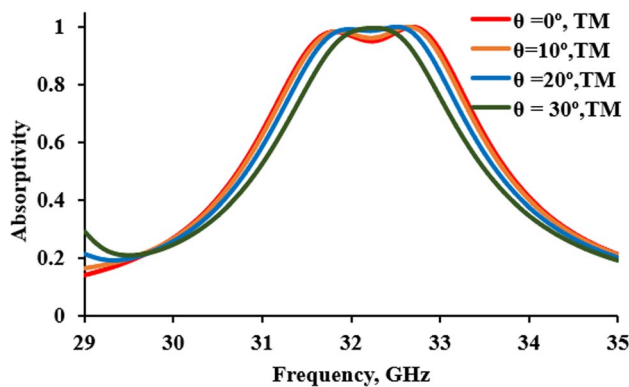**Fig. 15** Simulated absorption characteristics for various oblique incidences under TE mode

Fig. 16 Simulated absorption characteristics for various oblique incidences under TM mode

5 Conclusion

This paper presented the design and characterization of a millimeter wave absorber. The proposed absorber is constructed using two concentric square rings with corrugations in between the square rings. The polarization stability characteristics are evaluated and presented. The proposed absorber has 95–100% absorptivity in the frequency range of 31.4–33.04 GHz. The bandwidth of 1.64 GHz, is achieved which equals 5% of the fractional bandwidth. The parametric analysis and surface current distribution for the bandwidth are analyzed and the results are presented in this work. Further, the proposed absorber is fabricated and the performance is measured. The results show that the measured and simulated absorption characteristics are similar. Thus, the proposed mm-wave absorber will be a better choice for RADAR and stealth applications.

References

1. T.Q. Van Hoang, B. Loiseaux, in *European Conference on Antennas and Propagation (EuCAP)* (2020), pp. 1–4
2. J.-J. Ma, W.H. Tong, K. Shi, X.-Y. Cao, B. Gong, Prog. Electromagn. Res. Lett. **49**, 73–78 (2014)
3. S. Fan, Y. Song, Materials (Basel) **13**, 21 (2020)
4. S.J. Li, P.X. Wu, H.X. Xu et al., Nanoscale Res. Lett. **13**, 386 (2012)
5. R.M.H. Bilal et al., IEEE Access **9**, 5670–5677 (2021)
6. N.I. Landy, S.S. Sajuyigbe, J.J. Mock, D.R. Smith, W.J. Padilla, Phys. Rev. Lett. **1**, 207–210 (2008)
7. W. Xin, Z. Binzhen, W. Wanjun, W. Junlin, D. Junping, IEEE Photonics J. **9**, 1–13 (2016)
8. P. Gao, W. Dou, L. Ye, in *Progress in Electromagnetics Research Symposium* (2017), pp. 1751–1755
9. A. Khoshniat, R. Abhari, IEEE Trans. Electromagn. Compat. **64**, 1314–1321 (2019)
10. J.C. Sten, P.K. Koivisto, IEEE Trans. Electromagn. Compat. **50**, 1011–1014 (2008)
11. E.F. Knott, C.D. Lunden, IEEE Trans. Antennas Propag. **43**, 1339–1343 (1995)
12. J. Li, Y. Yuan, G. Yang, Q. Wu, W. Zhang, S.N. Burokur, K. Zhang, Laser Photonics Rev. **17**, 2200777 (2023)
13. J.D. Ryder, Networks Lines and Fields II Ed., Pearson, 2015
14. B.A. Munk, Frequency Selective Surfaces: Theory and Design, Wiley, 2000
15. D.Y. Shchegolkov, A.K. Azad, J.F. O'Hara, E.I. Simakov, Phys. Rev. B Condensed Matter, **82** (2010)
16. A. Veeraselvam, G.N.A. Mohammed, K. Savarimuthu, P.D. Vijayaraman, IEEE Sens. J. **22**, 2045–2052 (2022)
17. K. Singh, M.P. Abegaonkar, S.K. Koul, IEEE Trans. Electromagn. Compat. **61**, 877–886 (2012)
18. H.T. Yudistira, K. Kananda, J. Electron. Mater. **50**, 389–396 (2021)
19. J.C. Iriarte Galarregui, A. Tellechea Pereda, J.L.M. de Falcón, I. Ederra, R. Gonzalo, P. de Maagt, IEEE Trans. Antennas Propag. **61**, 6136–6143, (2013)
20. M. Paquay, J.-C. Iriarte, I. Ederra, R. Gonzalo, P. de Maagt, IEEE Trans. Antennas Propag. **55**, 3630–3638 (2007)
21. W. Yuan, Y. Cheng, Appl. Phys. A **117**, 1915–1921 (2014)
22. Y. Cheng, Y. Nie, R. Gong, Appl. Phys. B **111**, 483–488 (2013)
23. Y.Z. Cheng, Y. Wang, Y. Nie, R.Z. Gong, X. Xiong, X. Wang, J. Appl. Phys. **111**, 044902 (2012)
24. Z. Miao, C. Huang, Q. Zhao, M. Pu, X. Ma, X. Luo, in *International Conference on Microwave and Millimeter Wave Technology (ICMMT)* (2012), p. 6230429
25. S. Pandit, A. Mohan, P. Ray, in *IEEE MTT-S International Microwave and RF Conference (IMaRC), 1* (2018), p. 3
26. J. Dong et al., Micromachines **12**, 1–5 (2021)
27. A. Musa, M.L. Hakim, T. Alam, M.H. Baharuddin, M.S.J. Singh, in *7th International Conference on Space Science and Communication (IconSpace)* (2021), pp. 151–155
28. S. An, Xu. Haibing, Y. Zhang, Wu. Song, J. Jiang, Y. He, L. Miao, J. Appl. Phys. **122**, 025113 (2017)